Available online at www.sciencedirect.com

SciVerse ScienceDirect

Procedia Engineering 00 (2015) 000–000

Procedia Engineering

www.elsevier.com/locate/procedia

24th International Meshing Roundtable (IMR24)

Handling Extraordinary Nodes with Weighted T-spline Basis Functions

Lei Liu, Yongjie Jessica Zhang*, Xiaodong Wei

Department of Mechanical Engineering, Carnegie Mellon University, Pittsburgh, PA 15213, USA

Abstract

To generate analysis-suitable T-splines for arbitrary topologies, in this paper we introduce a new method to deal with extraordinary nodes in the T-mesh. Knot interval duplication method is used to extract knot vectors for the extraordinary nodes and spoke nodes. From defined bicubic weighted T-spline basis functions, the extracted Bézier coefficients are modified to obtain a gap-free T-spline surface. The boundaries shared by the first-ring neighboring Bézier elements are C^0-continuous. Then we use biquartic Bézier basis functions with optimized coefficients to increase the surface continuity to G^1. Comparison with other methods shows that our method generates T-spline surfaces with better surface continuity for analysis.

Peer-review under responsibility of organizing committee of the 24th International Meshing Roundtable (IMR24).

Keywords: Extraordinary Nodes, Surface Continuity, Weighted T-spline Basis, Degree Elevation, Isogeometric Analysis

1. Introduction

Isogeometric analysis was developed to integrate design with analysis, which uses the same basis functions for geometrical representation and numerical simulation [1]. Compared to traditional finite element method, it has the superior performance in accuracy and robustness [2–4]. Isogeometric analysis has been studied in different perspectives and application fields, such as linear elastics [1,5,6], fluid-structure interaction [7–9], structure vibrations [10], and electromagnetics [11], demonstrating the advantages of this new analysis method.

NURBS (Non-Uniform Rational B-splines) [1,4,12] and T-splines [13,14] are two techniques popularly used in isogeometric analysis. Compared to NURBS, the main advantage of T-splines is that T-splines allow T-junctions in the control mesh, and extraordinary nodes can be introduced to one single T-spline patch. Thus T-splines support local refinement and arbitrary topologies. However, extraordinary nodes bring trouble to the basis definition in their neighborhood. Subdivision basis functions [13] and T-spline basis functions defined on knot vectors with duplicated knots [15] have been used to calculate the surface around the extraordinary nodes. For bicubic T-splines, the surface continuity around the extraordinary nodes is decreased to C^0 or G^1.

Different methods have been developed to handle extraordinary nodes on T-spline surfaces. Templates were developed in [15], with zero-length edges inserted around the extraordinary nodes to generate gap-free T-spline surfaces.

*Corresponding author: Yongjie Jessica Zhang, Tel: (412) 268-5332; Fax: (412) 268-3348.
E-mail address: jessicaz@andrew.cmu.edu

1877-7058
Peer-review under responsibility of organizing committee of the 24th International Meshing Roundtable (IMR24).

The surface continuity is C^0-continuous within two-ring neighborhood of the extraordinary nodes. This template method was further extended to volumetric T-spline modeling [16]. A capping method [17] calculates the Bézier control points from T-spline control points to obtain a G^1-continuous T-spline surface around the extraordinary nodes. However, the Bézier extraction matrix cannot be obtained. Standard T-splines with an optimization scheme was developed to support extraordinary nodes in isogeometric boundary element analysis [5], as well as fluid-structure interactions with hybrid variational-collocation immersed method [18]. A linear interpolation scheme was first developed to obtain Bézier extraction matrix from T-meshes, and then the extracted Bézier element coefficients were optimized to obtain G^1 continuity around extraordinary nodes. Isogeometric spline forests were proposed to represent surfaces and volumes of arbitrary topologies with hierarchical splines. The first-ring neighborhood of extraordinary nodes is represent with C^0 forest formed by spline trees with connected control points [19]. Subdivision basis functions can also be used to deal with extraordinary nodes. Truncated hierarchical Catmull-Clark basis functions were used around the extraordinary nodes [20], where the resulting surface is C^1-continuous. In geometric design, higher degree basis functions were used sometimes for better smoothness, such as using biquintic basis functions to get C^1-continuous surfaces [21], and even G^2-continuous surfaces [22,23].

In this paper, we present a new knot interval duplication and optimization method to deal with extraordinary nodes. Knot intervals influenced by the extraordinary nodes are assigned with a designated duplication method. Weighted T-spline basis functions are defined on the designed knot vectors. With the proposed method, the obtained surface is C^0-continuous across the boundary shared by first-ring neighborhood Bézier elements, C^1-continuous across the boundary shared by first-ring and second-ring Bézier elements, and C^2-continuous everywhere else. Degree elevation is then performed to obtain biquartic Bézier coefficients within the first-ring neighborhood. An optimization procedure is used to recalculate the coefficients, ensuring that the first-ring Bézier elements are G^1-continuous.

The remainder of this paper is as follow. The weighted T-spline basis is reviewed in Section 2. We discuss the detailed algorithm to handle extraordinary nodes in Section 3. The comparison of different methods dealing with extraordinary nodes are given in Section 4, together with results of four different models. The conclusion is drawn in Section 5 with the future work.

2. A Brief Review of Weighted T-splines

For details of T-splines and their application in analysis, we suggest readers to refer to [14]. Here we clarify several necessary terminologies. *T-mesh* is the control mesh of a T-spline with all the topological information. For each vertex in the T-mesh, local *knot vectors* are inferred by shooting rays [24], based on which the corresponding T-spline basis functions are defined. T-mesh allows *T-junctions* and extraordinary nodes. T-junctions are analogous to the hanging nodes in classical finite elements. An extraordinary node is an interior vertex (not a T-junction) with valance other than 4. T-junctions are extended to obtain the *elemental T-mesh*. We can extract one Bézier element from each elemental T-mesh element.

There are different types of T-splines, and only a restricted subset can be used in analysis. The definition and linear independence of analysis-suitable T-spline basis functions of arbitrary degree were studied in [25]. Partition of unity and linear independence properties are prerequisites of T-spline basis functions for analysis. Analysis-suitable T-splines have certain constraints on the T-mesh [26]. To ensure the constructed T-spline is analysis-suitable, the T-junction extensions from two different parametric directions cannot intersect with each other. An extension algorithm was also introduced to generate T-meshes which result in analysis-suitable T-splines. Strongly-balanced quadtree and octree T-meshes were used in the construction of polynomial spline spaces, and the defined cubic T-spline basis functions can be used in analysis [27]. Instead of performing T-junction extensions, modified T-splines recalculate the T-spline basis functions [28]. The modified T-splines also satisfy linear independence and partition of unity properties. Hierarchical analysis-suitable T-splines were also proposed with highly localized refinement algorithms, and were utilized in adaptive isogeometric analysis [29].

The weighted T-spline was introduced in [30], which has less topological constraint over the T-mesh. T-junction extension is not necessary for weighted T-splines. Given a basis function $N^r(\xi,\eta)$ defined on locally subdivided T-mesh without T-junction extension, refinability indicates

$$N^r(\xi,\eta) = \sum_q c_q^r N_q^c(\xi,\eta), \tag{1}$$

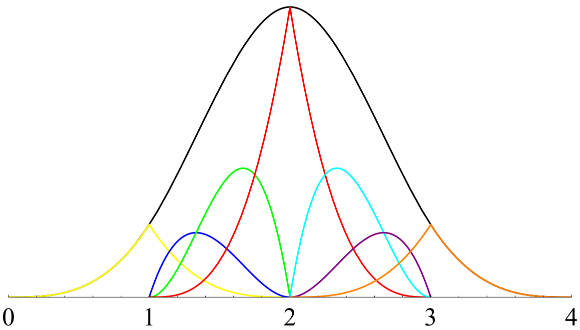

Fig. 1. T-spline basis function $N(\xi)$ (the black curve) defined on the knot vector $\{0, 1, 2, 3, 4\}$ and the extracted seven weighted Bézier basis functions (curves rendered with different colors). The seven weighted Bézier basis functions are defined on $\{0, 1, 1, 1, 2\}$, $\{1, 1, 1, 2, 2\}$, $\{1, 1, 2, 2, 2\}$, $\{1, 2, 2, 2, 3\}$, $\{2, 2, 2, 3, 3\}$, $\{2, 2, 3, 3, 3\}$ and $\{2, 3, 3, 3, 4\}$, and the weights are $1/6, 1/3, 2/3, 2/3, 2/3, 1/3$ and $1/6$, respectively.

where $N_q^c(\xi, \eta)$ is the qth children basis function of $N^r(\xi, \eta)$. Here a children basis function refers to a basis function defined on the refined knot vectors, which can be obtained by inserting knots to the knot vectors of $N^r(\xi, \eta)$. Note that with $N^r(\xi, \eta)$ and quadtree subdivision local refinement, partition of unity may not be satisfied everywhere [30]. So the corresponding weighted T-spline basis function with respect to $N^r(\xi, \eta)$ is defined as

$$N^w(\xi, \eta) = \sum_q h_q N_q^c(\xi, \eta), \tag{2}$$

where h_q are weighting coefficients, or the new weights of the children basis functions. h_q can be obtained by enforcing partition of unity satisfied everywhere. Weighted T-spline basis functions are linearly independent and meet all the requirements of isogeometric analysis [30].

Based on the Bézier extraction algorithm [24], $N^r(\xi, \eta)$ can also be represented as a linear combination of Bézier basis functions. We have

$$N^r(\xi, \eta) = \sum_i c_i B_i(\xi, \eta), \tag{3}$$

where c_i are the Bézier extraction coefficients, or weights, and $B_i(\xi, \eta)$ are Bézier basis functions. c_i can be obtained from the knot insertion algorithm [31]. To explain Bézier extraction, a T-spline basis function $N(\xi)$ together with seven extracted Bézier basis functions are shown in Fig. 1. $N(\xi)$ is defined on knot vector $\{0, 1, 2, 3, 4\}$. Seven Bézier basis functions can be extracted from $N(\xi)$, defined on knot vectors $\{0, 1, 1, 1, 2\}$, $\{1, 1, 1, 2, 2\}$, $\{1, 1, 2, 2, 2\}$, $\{1, 2, 2, 2, 3\}$, $\{2, 2, 2, 3, 3\}$, $\{2, 2, 3, 3, 3\}$, and $\{2, 3, 3, 3, 4\}$ respectively.

Analogous to the weight recalculating method to enforce partition of unity [30], a different weighted T-spline basis function can be defined by recalculating the weights of extracted Bézier basis functions. So the corresponding weighted T-spline of $N^r(\xi, \eta)$ can be represented as

$$\hat{N}^w(\xi, \eta) = \sum_i \hat{c}_i B_i(\xi, \eta), \tag{4}$$

where $\hat{c}_i$ are the modified weightes. Eqn. (4) will be used to define weighted T-spline basis functions to deal with extraordinary nodes, and we will discuss how to compute $\hat{c}_i$ in Section 3.

3. Weighted T-spline Surface Calculation

To obtain gap-free T-spline surfaces of arbitrary topologies, handling extraordinary nodes of the T-mesh is a prerequisite. In this section, we first introduce a new knot interval duplication method to assign knot interval vectors to vertices. Based on the assigned knot interval vectors, bicubic T-spline basis functions are defined, and a gap-free weighted T-spline surface is obtained. Then surface continuity elevation is performed to ensure that the extracted first-ring Bézier elements are G^1-continuous.

3.1. Topological Constraints and Knot Interval Duplication

A local knot interval vector in the ξ direction is a sequence of knot intervals $\Delta\Xi = \{\Delta\xi_1, \Delta\xi_2, \cdots, \Delta\xi_{p+1}\}$, and its corresponding knot vector is a non-decreasing knot sequence $\Xi = \{\xi_1, \xi_2, \cdots, \xi_{p+2}\}$ such that $\Delta\xi_i = \xi_{i+1} - \xi_i$. Each vertex in the T-mesh is assigned with a knot interval vector along each parametric direction, based on which knot vectors and T-spline basis functions are defined. For vertices near extraordinary nodes, knot intervals cannot be directly obtained in the canonical way. Here we develop a new method to assign knot intervals to such vertices. Necessary terminologies are defined first to assist our explanation.

A *spoke edge* is an edge touching an extraordinary node. A *spoke node* is the vertex other than the extraordinary node on a spoke edge. All the other nodes besides extraordinary nodes and spoke nodes in the T-mesh are *regular nodes*. For a first-ring neighboring T-mesh element of an extraordinary node, the only regular node in this element is a *corner node*. For example in Fig. 2(a), the red circle is an extraordinary node, the green circle is a spoke node, and the black circle is a corner node. Three topological constraints are applied to the local region around the extraordinary nodes:

(1) No other extraordinary nodes are allowed within the four-ring neighborhood of an extraordinary node;
(2) No T-junctions are allowed within the four-ring neighborhood of an extraordinary node; and
(3) The knot intervals of all the spoke edges of an extraordinary node are non-zero.

These topological constraints are the foundation of our method to obtain a gap-free T-spline surface. They ensure that the resulting T-spline surface around an extraordinary node is not influenced by other extraordinary nodes or T-junctions. For elements beyond the two-ring neighborhood of any extraordinary node, we assume analysis-suitable requirements are satisfied, and weighted T-spline basis functions [30] are employed to calculate analysis-suitable T-splines.

To define T-spline basis functions of degree p, each vertex in the T-mesh is assigned with a pair of local knot interval vectors to define their local knot vectors. How to extract knot intervals from the T-mesh was explained in [24]. For each vertex, we shoot rays in each parametric direction until $p-1$ vertices or perpendicular edges are intersected. A knot interval is the parametric distance between two consecutive intersections. Thus we obtain a knot interval vector in each direction. Zero knot intervals are appended when a boundary is crossed before $p-1$ intersections are found. However, this method fails when the ray encounters an extraordinary node before $p-1$ intersections. The reason is that the parametric direction cannot be determined for the ray. In [15], zero knot intervals are appended for this situation, resulting in repeated knots in the knot vectors.

Here we explain our interval duplication method to assign knot intervals to the vertices, which is based on the ray-shooting method. The basic idea is to set the current knot interval equal to the previous one whenever the ray encounters an extraordinary node. There are three different cases.

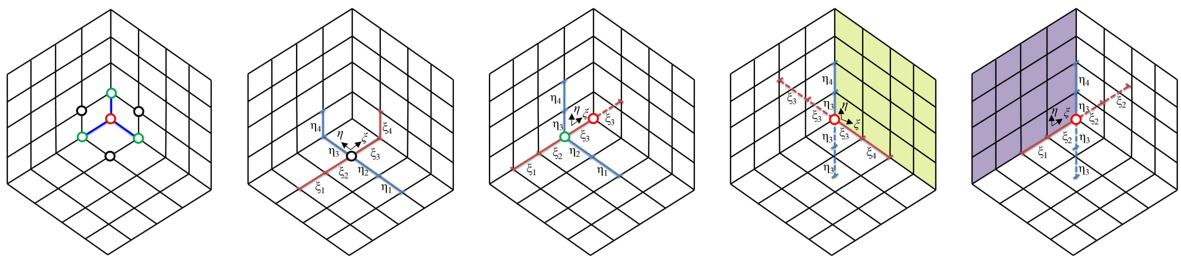

(a) (b) (c) (d) (e)

Fig. 2. Knot interval extraction near the extraordinary node. (a) Corner nodes (the black circles), spoke nodes (the green circles), extraordinary node (the red circle) and spoke edges (the blue edges) in the T-mesh configuration; (b) corner node with ordinary knot intervals; (c) spoke node with extended knot intervals; (d) extraordinary node with knot intervals duplicated with respect to elements in the green region; and (e) the same extraordinary node with knot intervals duplicated with respect to the elements in the purple region.

Regular Node (Case 1). Knot intervals are extracted by shooting rays in each parametric direction. They are not influenced by the extraordinary nodes. For example, the extracted knot interval vectors for the regular node (the black circle) in Fig. 2(b) are $\{\xi_1, \xi_2, \xi_3, \xi_4\}$ and $\{\eta_1, \eta_2, \eta_3, \eta_4\}$.

Spoke Node (Case 2). Interval duplication is used in this case. When the ray encounters an extraordinary node, it stops. For non-determined interval, we set it equal to the previous interval. For example for the spoke node (the green circle) in Fig. 2(c), the first three intervals are found by the ray-shooting method, $\{\xi_1, \xi_2, \xi_3\}$. The ray stops at the extraordinary node (the red circle). We set the last interval equal to ξ_3. The full knot interval for this spoke node in ξ direction is $\{\xi_1, \xi_2, \xi_3, \xi_3\}$.

Extraordinary Node (Case 3). Similar to spoke nodes, the previous interval value is duplicated when an extraordinary node is encountered. The interval duplication depends on the local parametric directions. For example, the red circle is an extraordinary node in Fig. 2(d) and (e). For the elements in the green region with the given local coordinate system, the obtained knot intervals by shooting rays are $\{\xi_3, \xi_4\}$ and $\{\eta_3, \eta_4\}$. Via interval duplication, the final knot intervals for this extraordinary node are $\{\xi_3, \xi_3, \xi_3, \xi_4\}$ and $\{\eta_3, \eta_3, \eta_3, \eta_4\}$. For the elements in the purple region, the knot intervals of the same extraordinary node are $\{\xi_1, \xi_2, \xi_2, \xi_2\}$ and $\{\eta_3, \eta_3, \eta_3, \eta_4\}$.

Remark 3.1. The knot intervals are duplicated in such a way that there are no knots with the same value in the knot vectors, and the basis functions defined upon them are all cubic polynomials.

With the introduced interval duplication method, we define T-spline basis functions for all the vertices. For a vertex A, its associated basis function is denoted as N_A. If N_A has non-zero basis function value over the region covered by a T-mesh element, then N_A has support over the corresponding Bézier element. The support of an extraordinary node or a spoke node is its two-ring neighborhood. The number of T-spline basis functions that have support over the two-ring neighboring Bézier elements of an extraordinary node varies. For example for the element with a valance-3 extraordinary node in Fig. 3, 14 T-spline basis functions (marked with cyan circles) have support over the first-ring neighboring Bézier elements (light blue), shown in Fig. 3(a). For the second-ring neighboring elements like the light green elements in Fig. 3(b-c), 16 basis functions have support over it.

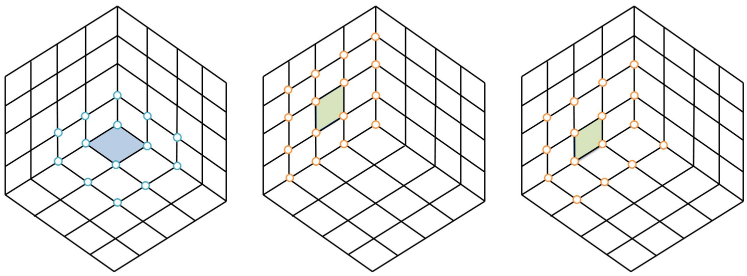

(a) (b) (c)

Fig. 3. Basis functions with support over a Bézier element. (a) For a Bézier element (light blue) in the first-ring neighborhood of an extraordinary node with valance-3, 14 basis functions (cyan circles) have support over it; and (b-c) for a Bézier element (light green) in the second-ring neighborhood, 16 basis functions (orange circles) have support over it.

Gap-free Requirement. For bicubic T-spline surfaces with extraordinary nodes, two-ring neighboring elements are influenced by the extraordinary nodes. For each influenced T-mesh element, only one Bézier element is extracted under the topological constraints given in Section 3.1. In the following when checking the T-spline surface continuity, we check the continuity across the boundary shared by the extracted Bézier elements. To obtain a gap-free surface, Bézier elements extracted from two adjacent first-ring neighborhood T-mesh elements should be at least C^0-continuous across the shared boundary. For example in Fig. 4, there is a valence-n extraordinary node P_E, n spoke nodes ($P_S^1 \sim P_S^n$) and n first-ring neighborhood elements. T-mesh element e^i and e^{i-1} share one spoke edge $P_E P_S^i$ (the red edge) in the T-mesh. The Bézier elements extracted from them need to meet along the shared boundary.

3.2. Gap-free Surface Calculation

For the region beyond the two-ring neighborhood of an extraordinary node, the knot interval extraction, T-spline basis definition and Bézier element extraction follow the canonical T-spline manner [24]. For the first-ring neighboring

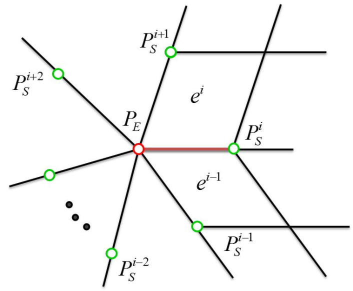

Fig. 4. Gap-free requirement for a T-mesh with an extraordinary node P_E and n spoke nodes P_S^i. Two first-ring neighborhood T-mesh elements e^{i-1} and e^i share one red edge, and their extracted Bézier elements should be gap-free along the shared boundary.

T-mesh elements, there are two steps to calculate the weighted T-spline surface and extract Bézier elements. For each Bézier element, we find T-spline basis functions with support on it based on the defined local coordinate system, and calculate the corresponding Bézier coefficients. Then the gap-free requirement is applied by modifying the Bézier coefficients.

Bézier Coefficient Calculation. Taking the valance-n extraordinary node P_E in Fig. 5(a) as an example, e^i is a first-ring neighborhood T-mesh element, and e_b^i is the Bézier element extracted from it; $P_E P_S^i$ is a spoke edge with edge interval a_i; P_C^i is the corner node of e_i. As shown in Fig. 5(b), we define the local parametric coordinate system of e_i by setting P_E as the origin, $P_E P_S^i$ following the ξ direction, $P_E P_S^{i+1}$ following the η direction, $P_E P_S^{i+2}$ following the $-\xi$ direction and $P_E P_S^{i-1}$ following the $-\eta$ direction. Then the spoke nodes $P_S^{i-1} \sim P_S^{i+2}$, the corner nodes $P_C^{i-2} \sim P_C^{i+1}$ are selected and assigned with parametric coordinates. All other spoke nodes and corner nodes are not assigned with parametric coordinates, even through their basis functions have support on e_b^i. The reason is that in the defined local parametric coordinate system, we cannot reach these nodes from the origin by moving along mesh edges following the ξ or η directions. Regular nodes with support over e_b^i are also assigned with local parametric coordinates.

There are 16 vertices assigned with parametric coordinates, shown in Fig. 5(a) with circles rendered in different colors. The red circle represents the extraordinary node; the green circles represent the selected spoke nodes; the purple circles represent the selected corner nodes and the orange circles represent the selected regular nodes. Based on the assigned knot intervals, we define local knot vectors and T-spline basis functions for the 16 selected vertices. The T-spline surface can be represented as

$$S^i = \sum_j P_j N_j(\xi,\eta) = \sum_j P_j \sum_{k=1}^{16} M_{j,k}^i B_k(\xi,\eta) = \mathbf{P}_i^T \mathbf{M}^i \mathbf{B} = \sum_{k=1}^{16} Q_k^i B_k(\xi,\eta), \tag{5}$$

where P_j are the selected vertices (or control points), $N_j(\xi,\eta)$ are the corresponding T-spline basis functions which have support over e^i, $B_k(\xi,\eta)$ are Bézier basis functions, $M_{j,k}^i$ is the Bézier extraction matrix obtained from Eqn. (3), and Q_k^i are the Bézier control points. Here S^i denotes the T-spline surface calculated from e^i. We have

$$Q_k^i = \sum_j P_j M_{j,k}^i. \tag{6}$$

Let $k = \alpha \times 4 + \beta$, Eqn. (5) is rewritten as

$$S^i = \sum_{k=1}^{16} Q_k^i B_k(\xi,\eta) = \sum_{\alpha=1}^{4}\sum_{\beta=1}^{4} Q_{\alpha\beta}^i B_{\alpha\beta}(\xi,\eta). \tag{7}$$

Each Bézier control point $Q_{\alpha\beta}^i$ has a corresponding overall coefficient

$$c_{\alpha\beta}^i = \sum_j M_{j,\alpha\times4+\beta}^i. \tag{8}$$

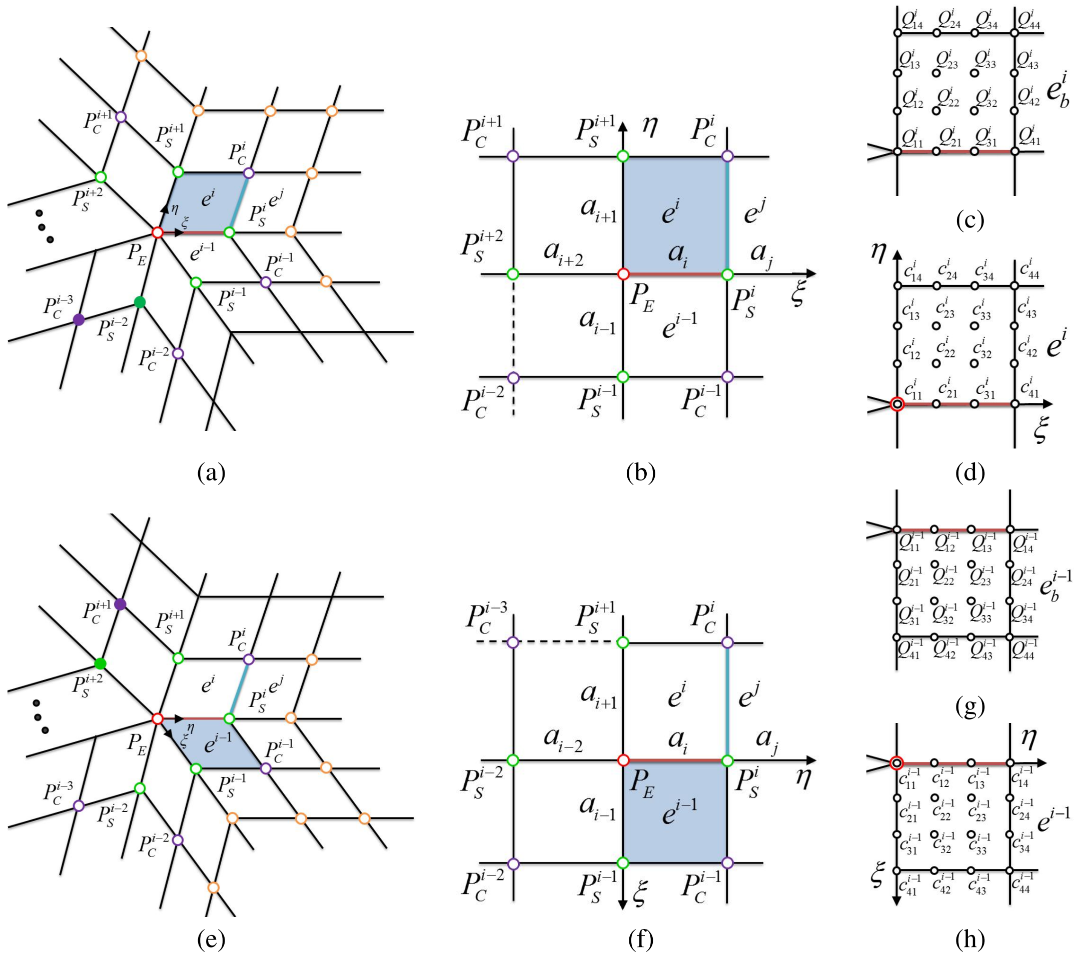

Fig. 5. Local parametric coordinate system, selected supporting T-spline basis functions, the order of calculated Bézier control points and coefficients for T-mesh element e^i and e^{i-1}. (a) T-mesh element e^i with its selected basis functions marked with circles. Red, green, purple and orange circles represent selected basis functions defined on the extraordinary node, spoke nodes, corner nodes and regular nodes, respectively; (b) the local parametric coordinate system of e^i, where a_i represent the assigned intervals to the edges; (c) the order of calculated control points of Bézier element e^i_b extracted from e^i; (d) the overall coefficient order of e^i_b; (e) element e^{i-1} with its selected basis functions; (f) the local coordinate system of e^{i-1}; (g) the order of control points of Bézier element e^{i-1}_b extracted from e^{i-1}; and (h) the overall coefficient order of e^{i-1}_b.

$Q^i_{\alpha\beta}$ have the same order with $c^i_{\alpha\beta}$, as shown in Fig. 5(c) and (d), respectively.

Similarly for element e^{i-1}, which shares the spoke edge $P_E P^i_S$ with e^i, its local parametric coordinate system, the selected T-spline basis functions, the order of Bézier control points and the overall Bézier coefficients are shown in Fig. 5(e-h). The spoke node P^{i-2}_S and the corner node P^{i-3}_C (marked with solid dots in Fig. 5(a)) are not selected for e^i to assign with local parametric coordinates. But they are selected for e^{i-1}. Similarly, P^{i+2}_S and P^{i+1}_C are selected for e^i, but not for e^{i-1}.

Note that if P_E is valance-3, P^{i+2}_S and P^{i-1}_S coincide. This means that in e^i, P^{i-1}_S is assigned with two local parametric coordinates, $(0, -a_{i-1})$ and $(-a_{i+2}, 0)$, to obtain the knot vectors. There are two basis functions defined on P^{i-1}_S. With this duplication, we can always define 16 T-spline basis functions with support over one first-ring element. In addition, we have the following proposition.

Proposition 3.1. *The Bézier elements extracted from the first-ring T-mesh elements do not meet with its adjacent first-ring neighbors.*

Proof. Bézier elements e_b^i and e_b^{i-1} are extracted from e^i and e^{i-1} respectively. Assume they meet along the shared boundary, then we have

$$Q^i_{\alpha 1} = Q^{i-1}_{1\alpha}, \quad 1 \le \alpha \le 4. \tag{9}$$

Based on the local parametric coordinate system of e^i and e^{i-1}, vertices P_S^{i+2} and P_C^{i+1} (marked with empty circles in Fig. 5(a) and solid dots in Fig. 5(e)) have contribution to Q^i_{11}, but not to Q^{i-1}_{11}. P_S^{i-2} and P_C^{i-3} (marked with solid dots in Fig. 5(a) and empty circles in Fig. 5(e)) have contribution to Q^{i-1}_{11}, but not to Q^i_{11}. Then $Q^i_{11} \neq Q^{i-1}_{11}$, which contradicts the assumption of meeting along the shared boundary. Thus, we prove this proposition. □

Bézier Coefficient Modification. We modify the Bézier coefficients to make the resulting T-spline surface gap-free. Based on the local coordinate systems and assigned knot intervals, it is easy to obtain that P_S^{i+2} and P_C^{i+1} only contribute to Q^i_{11}, while P_S^{i-2} and P_C^{i-3} only contribute to Q^{i-1}_{11}. So we have

$$Q^i_{\alpha 1} = Q^{i-1}_{1\alpha}, \quad 2 \le \alpha \le 4. \tag{10}$$

We only need to modify Q^i_{11} and Q^{i-1}_{11} to ensure e_b^i and e_b^{i-1} meet along their shared boundary. From Eqn. (5), suppose the contribution of N_S^{i+2} and N_C^{i+1} to c^i_{11} are $M^i_{I(N_S^{i+2}),1}$ and $M^i_{I(N_C^{i+1}),1}$ respectively. The contribution of N_S^{i-2} and N_C^{i-3} to c^{i-1}_{11} are $M^{i-1}_{I(N_S^{i-2}),1}$ and $M^{i-1}_{I(N_C^{i-3}),1}$ respectively, where $I(N_j)$ is the mapping of the basis function N_j to its local index in Eqn. (5). Q^i_{11} and Q^{i-1}_{11} should be modified as

$$Q^i_{11} = Q^i_{11} + P_S^{i-2} M^{i-1}_{I(N_S^{i-2}),1} + P_C^{i-3} M^{i-1}_{I(N_C^{i-3}),1}, \tag{11}$$

and

$$Q^{i-1}_{11} = Q^{i-1}_{11} + P_S^{i+2} M^{i}_{I(N_S^{i+2}),1} + P_C^{i+1} M^{i}_{I(N_C^{i+1}),1}. \tag{12}$$

This modification can be recognized as adding P_S^{i-2} and P_C^{i-3}, which were selected for e^{i-1} only, to the extraction of e_b^i. Similarly, P_S^{i+2} and P_C^{i+1} are added to the extraction of e_b^{i-1}.

Analogously, to constrain that all the first-ring Bézier elements meet at their shared corner, all the spoke nodes and corner nodes that are not selected for the extraction of e_b^i should be added back. Q^i_{11} is modified as

$$\bar{Q}^i_{11} = Q^i_{11} + \sum_{j=1, j\neq i}^{n} \bar{P}_{SC} M^j_{I(\bar{N}_{SC}),1}, \tag{13}$$

where $\bar{P}_{SC}$ are the basis functions defined on the corner nodes and the spoke nodes not selected in the Bézier extraction of e^i, and $\bar{N}_{SC}$ are the associated T-spline basis functions. Note that $\bar{Q}^i_{11}$ is constant for all the first-ring Bézier elements. In Eqn. (8), since only c^i_{11} and c^{i-1}_{11} are modified, $\mathbf{M}^i$ is modified by adding new rows with non-zero entry only at the first position.

Based on the assigned knot intervals and local coordinate systems, there are always 16 T-spline basis functions selected for the extraction of one Bézier element. All the 16 basis functions are defined on local knot vectors without repeating knots. The T-spline basis functions are linearly independent and satisfy partition of unity before coefficient modification. Then from Eqn. (5) and Theorem 1 in [32], $\mathbf{M}^i$ is in full-rank and $c^i_{11} = 1$. Only the extraordinary node, spoke nodes and corner nodes have contribution to c^i_{11}. After Bézier coefficient modification, c^i_{11} is changed to

$$\begin{aligned} \bar{c}^i_{11} &= c^i_{11} + \sum_{j=1, j\neq i}^{n} M^j_{I(\bar{N}_{SC}),1} = 1 + \sum_{j=1, j\neq i}^{n} M^j_{I(\bar{N}_{SC}),1} \\ &= M^i_{I(N_E),1} + M^i_{I(\tilde{N}_{SC}),1} + \sum_{j=1, j\neq i}^{n} M^j_{I(\bar{N}_{SC}),1} = M^i_{I(N_E),1} + \sum_{j=1}^{n} M^j_{I(N_{SC}),1} > 1, \end{aligned} \tag{14}$$

where N_E is the basis function at the extraordinary node P_E, $\tilde{N}_{SC}$ are the basis functions defined on the corner nodes and spoke nodes selected for e^i, and N_{SC} are the basis functions defined on all the spoke nodes and corner nodes. To enforce $\bar{c}^i_{11} = 1$, we let

$$\bar{c}^i_{11} = M^i_{I(N_E),1} + \gamma \sum_{j=1}^{n} M^j_{I(N_{SC}),1} = 1, \tag{15}$$

where

$$\gamma = \frac{1 - M^i_{I(N_E),1}}{\sum_{j=1}^{n} M^j_{I(N_{SC}),1}}. \tag{16}$$

Eqns. (15)-(16) are used to modify the first column of $\mathbf{M}^i$. In the following we check the continuity between the first-ring and second-ring neighboring Bézier elements.

Proposition 3.2. *The Bézier elements extracted from the first-ring and second-ring T-mesh elements are C^1-continuous across their shared boundary.*

Proof. In Fig. 5(a), T-mesh elements e^i and e^j share one cyan edge. Bézier elements e^i_b and e^j_b are extracted from them. For e^i_b, its first derivative at the boundary shared with e^j_b is $\frac{\partial b^i(\xi,\eta)}{\partial \xi}|_{\eta=1}$, or $b^i_\xi(\xi)$. We adopt the notation

$$\langle \delta_1, \delta_2, \cdots, \delta_{p+1} \rangle^p(\xi) = \sum_{k=1}^{p+1} \delta_k B^p_k(\xi), \tag{17}$$

where $B^p_k(\xi)$ is a Bernstein polynomial of degree p. Then we have

$$b^i_\xi(\xi) = 3\langle Q^i_{31} - Q^i_{41}, Q^i_{32} - Q^i_{42}, Q^i_{33} - Q^i_{43}, Q^i_{34} - Q^i_{44} \rangle^3(\xi). \tag{18}$$

Here we check the contribution from the extraordinary node P_E to $b^i_\xi(\xi)$. N_E is the basis function at the extraordinary node P_E. Since $\eta = 1$, we only check N_E in the ξ direction. Based on the local parametric coordinate system of e^i, the knot vector to define N_E in the ξ direction is $\{-2a_i, -a_i, 0, a_i, a_i + a_j\}$. From Eqns. (5), (6) and (18), the contribution of P_E to $b^i_\xi(\xi)$ is

$$3P_E\langle \tilde{c}^i_{31} - \tilde{c}^i_{41}, \tilde{c}^i_{32} - \tilde{c}^i_{42}, \tilde{c}^i_{33} - \tilde{c}^i_{43}, \tilde{c}^i_{34} - \tilde{c}^i_{44} \rangle^3(\xi), \tag{19}$$

where $\tilde{c}^i_{3\alpha}$ and $\tilde{c}^i_{4\alpha}$ are the contribution of N_E to $c^i_{3\alpha}$ and $c^i_{4\alpha}$ $(1 \le \alpha \le 4)$. In the ξ direction, Bézier basis functions $B_{1\alpha}$, $B_{2\alpha}$, $B_{3\alpha}$ and $B_{4\alpha}$ are defined on knot vectors $\{-a_i, 0, 0, 0, a_i\}$, $\{0, 0, 0, a_i, a_i\}$, $\{0, 0, a_i, a_i, a_i\}$, $\{0, a_i, a_i, a_i, a_i + a_j\}$, respectively. Based on knot insertion algorithm, we have $\tilde{c}^i_{3\alpha} = 2\tilde{c}^i_{4\alpha}$. Eqn. (19) changes to

$$-3\langle P_E\tilde{c}^i_{41}, P_E\tilde{c}^i_{42}, P_E\tilde{c}^i_{43}, P_E\tilde{c}^i_{44} \rangle^3(\xi). \tag{20}$$

The contribution of all other T-spline basis functions to $b^i_\xi(\xi)$ has the same expression. Based on Eqn. (6), Eqn. (18) changes to

$$b^i_\xi(\xi) = -3\langle Q^i_{41}, Q^i_{42}, Q^i_{43}, Q^i_{44} \rangle^3(\xi). \tag{21}$$

This method can also be used to obtain the the first derivative at the shared boundary from Bézier element e^j_b. For the local parametric coordinate system of e^j, P^i_S is set as the origin. Its two parametric directions follow the ξ and η directions of e^i. The first derivative at the boundary shared with e^i_b is $\frac{\partial b^j(\xi,\eta)}{\partial \xi}|_{\eta=0}$, or $b^j_\xi(\xi)$. We have

$$b^j_\xi(\xi) = -3\langle Q^j_{11}, Q^j_{12}, Q^j_{13}, Q^j_{14} \rangle^3(\xi). \tag{22}$$

Since $Q^i_{4\alpha} = Q^j_{\alpha 1}$ $(1 \le \alpha \le 4)$, we have $b^i_\xi(\xi) = b^j_\xi(\xi)$. Therefore e^i_b and e^j_b are C^1-continuous across the shared boundary. □

Note that Bézier coefficient modification only changes Q^i_{11}. The C^1 continuity between e^i and e^j remains the same after the modification. With the modified Bézier coefficients, the T-spline surface is defined as

$$S^i = \mathbf{P}^i\hat{\mathbf{M}}^i\mathbf{B}, \tag{23}$$

where P^i are the control points including all the spoke nodes and corner nodes, $\hat{\mathbf{M}}^i$ is the modified extraction matrix.

Remark 3.2. T-spline basis functions defined by the linear combination of Bézier basis functions with modified coefficients are still analysis-suitable. The new Bézier transformation matrix $\hat{\mathbf{M}}^i$ is obtained by first adding new rows with non-zero entry only at the first position with Eqn. (13). Then the first column of the resulting matrix is further modified based on Eqns. (15) and (16). These two matrix operations do not change the matrix rank. So $\hat{\mathbf{M}}^i$ is in full rank and the modified T-spline basis functions remain analysis-suitable.

For a second-ring neighboring Bézier element, there are always 16 T-spline basis functions with support over it, as shown in Fig. 3(b-c). We can define the local coordinate system, and each selected vertex is assigned with local parametric coordinates. The T-spline surface is calculated with Eqn. (5), and no Bézier coefficient modification is necessary. So the corresponding Bézier extraction over these elements is the same with the canonical manner. The resulting surface continuity of second-ring neighboring Bézier elements and beyond is C^2.

3.3. Surface Continuity Elevation

To obtain higher surface smoothness for the first-ring Bézier elements, we adopt the optimization method introduced in [5] to perform continuity elevation. The necessary and sufficient condition for two adjacent Bézier elements to be G^1-continuous is that they share the same tangent plane across the boundary [33]. Degree elevation is first performed to obtain biquartic Bézier coefficients. These coefficients are then optimized to satisfy the G^1 continuity requirement.

For an extraordinary node of valance-n, there are $20n + 1$ unique Bézier coefficients and $20n$ constraint equations derived to satisfy the G^1 continuity requirement. These constraint equations are used to assemble the constraint matrix $\mathbf{G}^i$ and the corresponding right hand side vector $\mathbf{g}^i$. Besides, there are $40n$ fairing equations to obtain the fairing matrix $\mathbf{F}^i$ and the right hand side vector $\mathbf{f^i}$. The detailed expressions of the constraint and fairing equations are given in [5]. We obtain the optimized Bézier coefficients by solving

$$\min \parallel \mathbf{F}^i \hat{\mathbf{c}}^i - \mathbf{f}^i \parallel_2, \tag{24}$$

where

$$\hat{\mathbf{c}}^i = \arg\min_j \parallel \mathbf{G}^j \hat{\mathbf{c}}^j - \mathbf{g}^j \parallel_2 . \tag{25}$$

The optimization procedure handles extraordinary nodes with different valance numbers correctly. In Fig. 6, a T-spline model with two extraordinary nodes of valance 3 and 5 is shown. The calculated T-spline surface is G^1-continuous across the red edges, C^1-continuous across the yellow edges, and C^2-continuous anywhere else.

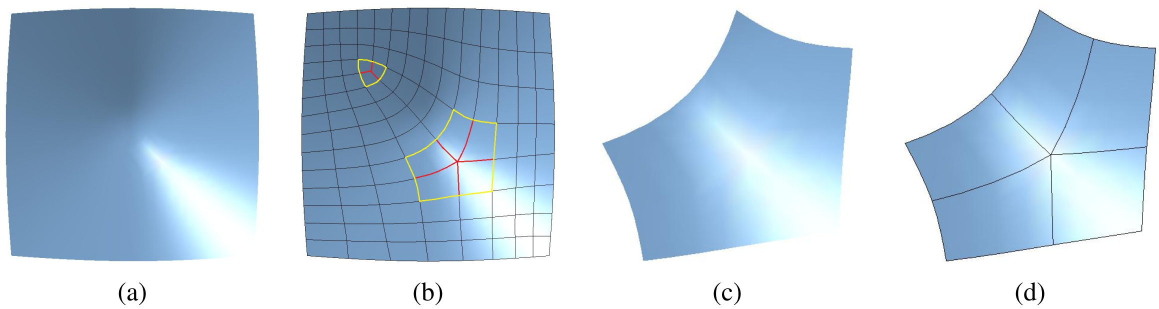

Fig. 6. Result of degree elevation for a T-spline model with two extraordinary nodes. (a) Calculated T-spline surface; (b) extracted Bézier elements, where red and yellow edges represent Bézier element boundaries with G^1-continuity and C^1-continuity across them respectively; (c) zoom-in of the first-ring neighborhood of the valance-5 extraordinary node; and (d) extracted Bézier elements of the first-ring neighborhood.

4. Results and Discussion

We compare our interval duplication algorithm with three other methods: the template method [15], the capping method [17], and the optimization method [5]. The surface continuity, Bézier extraction matrix, and T-mesh modification properties of these four methods are listed in Tab. 1.

Table 1. Comparison of four methods dealing with extraordinary nodes regarding surface continuity, Bézier extraction Matrix, and T-mesh modification.

Method	Surface Continuity across Red Edges in Fig. 6(b)	Surface Continuity across Yellow Edges in Fig. 6(b)	Surface Continuity 2*nd*-ring	Bézier Extraction Matrix Obtain Method	T-mesh Modification
Template	C^0	C^0	C^0	Knot Insertion	YES
Capping	G^1	C^1	C^1	NONE	NO
Optimization	G^1	C^1	C^1	Linear Interpolation	NO
Interval Duplication	G^1	C^1	C^2	Knot Insertion	NO

Template Method. Zero-interval edges are inserted around the extraordinary nodes [15], ensuring that the calculated T-spline surface is always gap-free. With this method, an extraordinary node can be within three-ring neighborhood of another one. But the drawback is that repeated knots are introduced to the knot vectors, and the surface continuity is C^0 between first-ring Bézier element pairs and second-ring Bézier element pairs. Furthermore, new control points are introduced for the insertion of zero-length intervals, which increases the total degrees of freedom for analysis.

Capping Method. The Bézier control points are directly calculated from T-spline control points [17]. They satisfy consistency conditions, resulting in G^1-continuous Bézier elements within the first-ring neighborhood. However, the transformation matrix from T-spline basis functions to Bézier basis functions cannot be obtained, which limits its direct usage in isogeometric analysis.

Optimization. The main difference between our method and the optimization method in [5] lies in the way to generate the gap-free T-spline surface before coefficient optimization. In the optimization method, a linear interpolation scheme is introduced to calculate Bézier control points from T-spline control points. Furthermore, the surface between the second-ring Bézier elements is C^2-continuous in our results, better than C^1-continuous from the optimization method.

From comparison we can conclude that our knot interval duplication method coupled with Bézier coefficients modification result in the best surface continuity within two-ring neighborhood. No T-mesh modification is needed for the initial Bézier extraction matrix calculation. The resulting T-spline can be directly used in isogeometric analysis.

We also tested our method on four models, including the Sphere, Eight, Tetra and Genus-three models, see Fig. 7. There are eight valance-3 extraordinary nodes on the Sphere model, eight valance-5 extraordinary nodes on the Eight model, eight valance-6 extraordinary nodes on the Tetra model, and four valance-8 extraordinary nodes on the Genus-three model. For each model, the final T-spline surface with extracted Bézier elements are shown first. Then it is followed by the zoom-in first-ring neighborhood of a selected extraordinary node. The surface rendering difference shows the surface change before and after degree elevation. The first-ring neighborhood Bézier elements are given in the end. Our method can handle extraordinary nodes with difference valance number correctly to generate gap-free T-spline surfaces. With Bézier coefficient optimization, the surface continuity is increased to G^1 within one-ring neighborhood.

5. Conclusion and Future Work

In conclusion, we have developed a new algorithm to handle extraordinary nodes with bicubic weighted T-spline basis functions. Duplicated knot intervals are used to define T-spline basis functions around extraordinary nodes. Surface continuity requirements are applied to recalculate Bézier coefficients. The extracted first-ring neighborhood Bézier elements are C^0-continuous across their shared boundaries. With biquartic Bézier coefficients and an optimization procedure, the surface continuity is elevated to G^1. T-splines with extraordinary nodes of various valance numbers are tested to show the robustness of the algorithm. The main limitation of our algorithm is that we require one extraordinary node cannot be within four-ring neighborhood of another one. So this method cannot work on T-meshes with adjacent extraordinary nodes. A given T-mesh should be pre-processed if there are extraordinary nodes disobeying this constraint. In the future, we plan to make the algorithm work on T-meshes with less constraints, and extend it to arbitrary degree T-spline surfaces with extraordinary nodes as well as volumetric T-splines.

Acknowledgements

This project was supported in part by the PECASE Award N00014-14-1–0234.

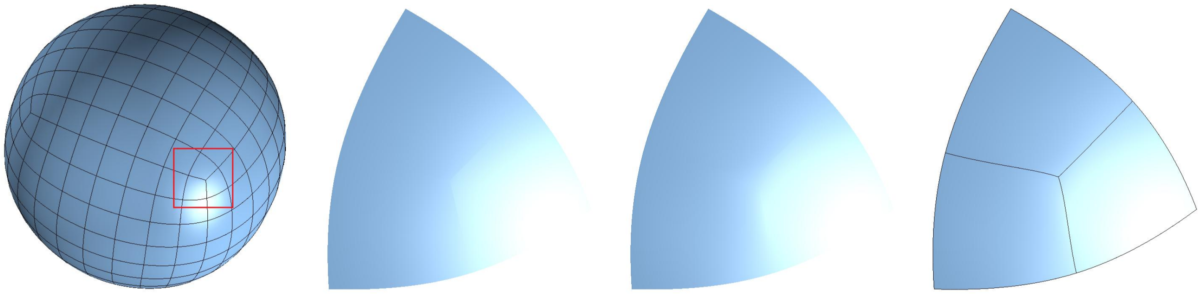

(a) Sphere model.

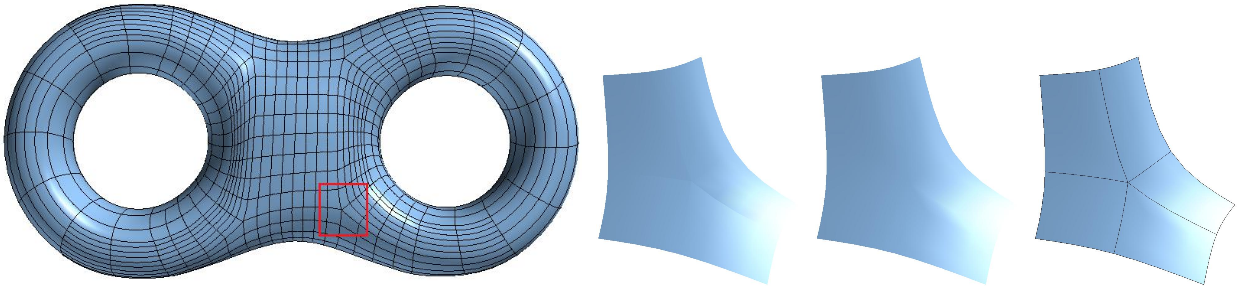

(b) Eight model.

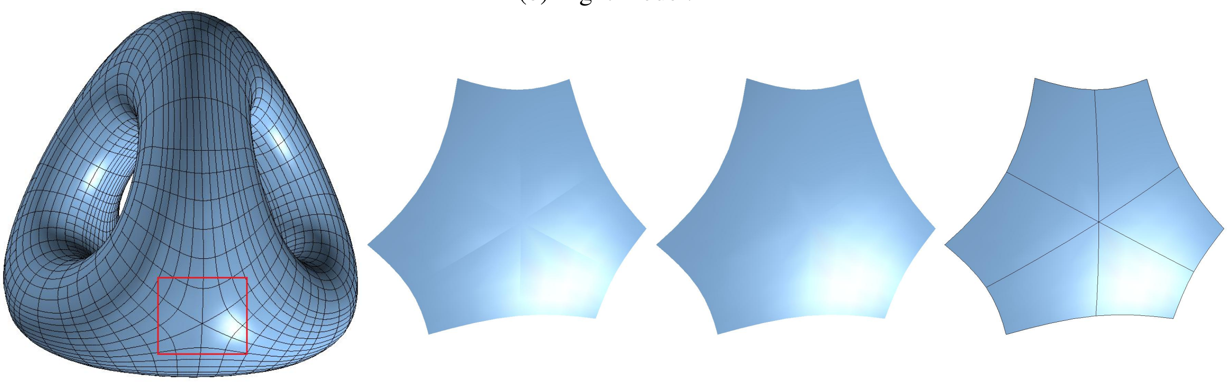

(c) Tetra model.

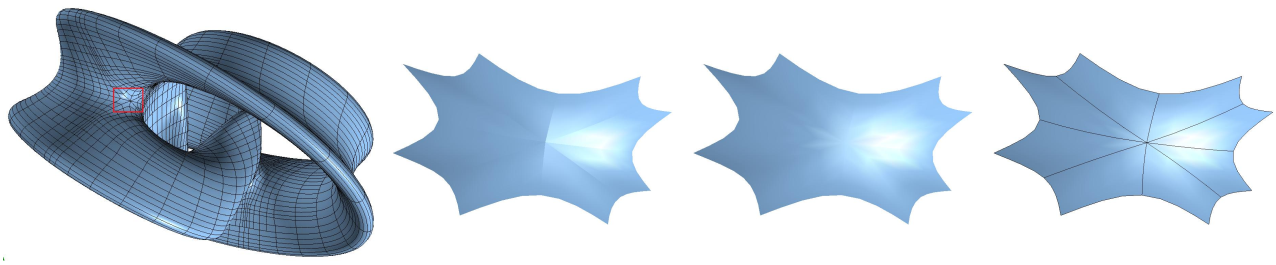

(d) Genus-three model.

Fig. 7. Calculated T-spline of four models. For each model, the final T-spline surface with extracted Bézier elements are shown first, followed by the zoom-in first-ring neighborhood of a selected extraordinary node before and after continuity elevation. The first-ring neighborhood Bézier elements are given in the end.

References

[1] T. J. R. Hughes, J. A. Cottrell, Y. Bazilevs, Isogeometric analysis: CAD, finite elements, NURBS, exact geometry, and mesh refinement, Computer Methods in Applied Mechanics and Engineering 194 (2005) 4135–4195.

[2] J. A. Cottrell, T. J. R. Hughes, Y. Bazilevs, Isogeometric analysis: toward integration of CAD and FEA, Wiley, 2009.

[3] Y. Bazilevs, I. Akkerman, D. J. Benson, G. Scovazzi, M. J. Shashkov, Isogeometric analysis of Lagrangian hydrodynamics, Journal of Computational Physics 243 (2013) 224–243.

[4] Y. Zhang, Y. Bazilevs, S. Goswami, C. L. Bajaj, T. J. R. Hughes, Patient-specific vascular NURBS modeling for isogeometric analysis of blood flow, Computer Methods in Applied Mechanics and Engineering 196 (2007) 2943–2959.

[5] M. A. Scott, R. N. Simpson, J. A. Evans, S. Lipton, S. P. A. Bordas, T. J. R. Hughes, T. W. Sederberg, Isogeometric boundary element analysis using unstructured T-splines, Computer Methods in Applied Mechanics and Engineering 254 (2013) 197–221.

[6] R. Dimitri, L. D. Lorenzis, M. A. Scott, P. Wriggers, R. L. Taylor, G. Zavarise, Isogeometric large deformation frictionless contact using T-splines, Computer Methods in Applied Mechanics and Engineering 269 (2014) 394–414.

[7] Y. Bazilevs, V. M. Calo, T. J. R. Hughes, Y. Zhang, Isogeometric fluid-structure interaction: theory, algorithms, and computations, Computational Mechanics 43 (2008) 3–37.

[8] Y. Bazilevs, V. M. Calo, Y. Zhang, T. J. R. Hughes, Isogeometric fluid-structure interaction analysis with applications to arterial blood flow, Computational Mechanics 38 (2006) 310–322.

[9] Y. Bazilevs, M.-C. Hsu, M. A. Scott, Isogeometric fluid-structure interaction analysis with emphasis on non-matching discretizations, and with application to wind turbines, Computer Methods in Applied Mechanics and Engineering 249-252 (2012) 28–41.

[10] J. A. Cottrell, A. Reali, Y. Bazilevs, T. J. R. Hughes, Isogeometric analysis of structural vibrations, Computer Methods in Applied Mechanics and Engineering 195 (2006) 5257–5296.

[11] A. Buffa, G. Sangalli, R. Vázquez, Isogeometric analysis in electromagnetics: B-splines approximation, Computer Methods in Applied Mechanics and Engineering 199 (2010) 1143–1152.

[12] G. Xu, B. Mourrain, R. Duvigneau, A. Galligo, Analysis-suitable volume parameterization of multi-block computational domain in isogeometric applications, Computer-Aided Design 45 (2013) 395–404.

[13] T. W. Sederberg, J. Zheng, A. Bakenov, A. Nasri, T-splines and T-NURCCs, ACM Transactions on Graphics 22 (2003) 477–484.

[14] Y. Bazilevs, V. M. Calo, J. A. Cottrell, J. A. Evans, T. J. R. Hughes, S. Lipton, M. A. Scott, T. W. Sederberg, Isogeometric analysis using T-splines, Computer Methods in Applied Mechanics and Engineering 199 (2010) 229–263.

[15] W. Wang, Y. Zhang, M. A. Scott, T. J. R. Hughes, Converting an unstructured quadrilateral mesh to a standard T-spline surface, Computational Mechanics 48 (2011) 477–498.

[16] W. Wang, Y. Zhang, G. Xu, T. J. R. Hughes, Converting an unstructured quadrilateral/hexahedral mesh to a rational T-spline, Computational Mechanics 50 (2012) 65–84.

[17] T. Sederberg, Bicubic capping with arbitrary knot intervals, Research Notes (2008).

[18] H. Casquero, L. Liu, C. Bona-Casas, Y. Zhang, H. Gomez, A hybrid variational-collocation immersed method for fluid-structure interaction using unstructured T-splines, International Journal for Numerical Methods in Engineering (2015) doi:10.1002/nme.5004 (2015).

[19] M. A. Scott, D. C. Thomas, E. J. Evans, Isogeometric spline forests, Computer Methods in Applied Mechanics and Engineering 269 (2014) 222–264.

[20] X. Wei, Y. Zhang, T. J. R. Hughes, M. A. Scott, Truncated hierarchical Catmull-Clark surface with local refinement, Computer Methods in Applied Mechanics and Engineering 291 (2015) 1–20.

[21] K. Karčiauskas, J. Peters, Point-augmented biquadratic C^1 subdivision surfaces, Graphical Models 77 (2015) 18–26.

[22] K. Karčiauskas, J. Peters, Biquintic surfaces via functionals, Computer Aided Geometric Design 33 (2015) 17–29.

[23] C. Loop, S. Schaefer, G^2 tensor product splines over extraordinary vertices, in: Proceedings of the Symposium on Geometry Processing, 2008, pp. 1373–1382.

[24] M. A. Scott, M. J. Borden, C. V. Verhoosel, T. W. Sederberg, T. J. R. Hughes, Isogeometric finite element data structures based on Bézier extraction of T-splines, International Journal for Numerical Methods in Engineering 88 (2011) 126–156.

[25] L. Beirão da Veiga, A. Buffa, G. Sangalli, R. Vázquez, Analysis-suitable T-splines of arbitrary degree: definition, linear independence and approximation properties, Mathematical Models and Methods in Applied Sciences 23 (2013) 1979–2003.

[26] M. A. Scott, X. Li, T. W. Sederberg, T. J. R. Hughes, Local refinement of analysis-suitable T-splines, Computer Methods in Applied Mechanics and Engineering 213-216 (2012) 206–222.

[27] M. Brovka, J. López, J. Escobar, J. Cascón, R. Montenegro, Construction of polynomial spline spaces over quadtree and octree T-meshes, Procedia Engineering 82 (2014) 21–33. 23rd International Meshing Roundtable (IMR23).

[28] H. Kang, F. Chen, J. Deng, Modified T-splines, Computer Aided Geometric Design 30 (2013) 827 – 843.

[29] E. J. Evans, M. A. Scott, X. Li, D. C. Thomas, Hierarchical T-splines: Analysis-suitability, Bézier extraction, and application as an adaptive basis for isogeometric analysis, Computer Methods in Applied Mechanics and Engineering 284 (2015) 1–20.

[30] L. Liu, Y. Zhang, X. Wei, Weighted T-splines with application in reparameterizing trimmed NURBS surfaces, Computer Methods in Applied Mechanics and Engineering 295 (2015) 108–126.

[31] R. Goldman, T. Lyche, Knot insertion and deletion algorithms for B-spline curves and surfaces, Society for Industrial and Applied Mathematics–Philadelphia, 1993.

[32] X. Li, J. Zheng, T. W. Sederberg, T. J. R. Hughes, M. A. Scott, On linear independence of T-spline blending functions, Computer Aided Geometric Design 29 (2012) 63–76.

[33] J. Zheng, G. Wang, Y. Liang, Curvature continuity between adjacent rational Bézier patches, Computer Aided Geometric Design 9 (1992) 321–335.